

Double differential inclusive hydrogen and helium spectra from neutron-induced reactions on carbon at 27.4, 39.7, and 60.7 MeV

T. S. Subramanian,* J. L. Romero, F. P. Brady, J. W. Watson,† D. H. Fitzgerald,‡
R. Garrett,§ G. A. Needham,|| J. L. Ullmann,¶ and C. I. Zanelli

Crocker Nuclear Laboratory and Department of Physics, University of California, Davis, California 95616

D. J. Brenner and R. E. Prael

Los Alamos National Laboratory, Los Alamos, New Mexico 87545

(Received 14 January 1983)

Double differential cross sections for the neutron-induced production of p, d, t, ^3He , and alpha particles from carbon have been measured using unpolarized neutrons. Neutron beam energies of 27.4, 39.7, and 60.7 MeV were used. The charged particle energy spectra at nine laboratory angles—15, 20, 35, 40, 45, 65, 90, 130, and 150 deg—range up to the kinematic maximum, from a lower energy cutoff of 4 MeV for p, d, t, and alpha and 8 MeV for ^3He . A CH target was used so that the absolute normalization was obtained simultaneously from the n-p cross sections. Intranuclear cascade plus deexcitation calculations were carried out. The data are compared with these calculations and with available proton induced (charge symmetric) reaction spectra.

[NUCLEAR REACTIONS $^{12}\text{C}(n,px;dx;^3\text{Hx};^3\text{Hex};^4\text{Hex})$, $E_n=27.4, 39.7, 60.7$
MeV; measured $\sigma(\theta;E)$, $\theta_{\text{lab}}=15, 20, 35, 40, 45, 65, 90, 130, 150$ deg. Intranuclear
cascade plus deexcitation calculations.]

I. INTRODUCTION

Extensive cross section data have been reported for neutron induced complex charged particle production around $E_n=14$ MeV.¹ However, data on carbon are limited to protons and alpha particles, since other channels are not accessible due to their high reaction Q values.² As the energy of the incident neutron is increased, the reactions for producing deuterons, tritons, and ^3He become energetically feasible. However, only total particle production cross section measurements have since been reported beyond the d - t neutron energies.³ We present here the first measurements of double-differential cross sections for hydrogen and helium isotope production from carbon at selected neutron energies in the 20–60 MeV range.

The data presented here are for incident neutron energies of 27.4, 39.7, and 60.7 MeV, which were chosen to facilitate comparison with the proton induced cross section measurements done at ORNL.⁴ Similar measurements on nitrogen and oxygen nuclei will be presented in subsequent publications.

The experimental setup is briefly discussed in Sec. II. Section III covers the format, normalization, corrections applied to the measured spectra, and the errors assigned to them. We introduce the model code, consisting of intranuclear cascade (INC) followed by Fermi breakup, which is used to generate predictions of double differential cross section spectra, in Sec. IV. Discussion of double differential cross section data along with comparisons with (i) the model predictions and (ii) the charge symmetric proton induced cross sections of Bertrand *et al.*⁴ is presented in Sec. V.

II. EXPERIMENTAL DETAILS

A nearly monochromatic neutron beam in the 20–60 MeV energy range was produced via the $^7\text{Li}(n,p)^7\text{Be}$

($Q=-1.64$ MeV) reaction.⁶ The neutrons were collimated along 0 degrees to strike a target located in an evacuated scattering chamber (Fig. 1). The neutron spectrum consists of a peak that contains $\cong 60\%$ of the neutrons plus a rather flat low energy tail (Fig. 2). For a typical 40 MeV, 14 μA proton beam, the intensity at 3.4 m is $\cong 10^5$ neutrons/cm² in a 1 MeV FWHM peak. Three sets of three-element charge particle telescopes located inside the chamber viewed the target at selected angles.

A polystyrene (CH) instead of elemental carbon was used as a target.⁷ This facilitates the normalization of data to the n-p elastic cross section that was measured simultaneously. By way of striking a compromise between viable count rates and minimum energy cutoff for alphas, target thicknesses in the 4–5 mg/cm² range were chosen. The actual target used for carbon consisted of four sheets of CH amounting to a thickness of 4.108 ± 0.054 g/cm². The target was oriented at 45 degrees to the incident beam so as to minimize the effective target thickness crossed by the outgoing charged particles towards either the forward angle telescopes or the backward angle telescope.

Three-element, charged particle detector telescopes consisting of a 50 μm Si (surface barrier) $\Delta E1$ detector, a 300–400 μm Si (surface barrier) $\Delta E2$ detector and a stopping E detector [NaI(Tl) or Si(Li)] were used for charged particle identification. Three such telescopes were positioned to cover, in all, nine laboratory angles, viz. 15, 20, 35, 40, 45, 65, 90, 130, and 150 degrees. Combinations of ΔE vs E displays for energetic particles and particle velocity (time of flight) vs E displays for particles that stopped in the first detector element were used to identify charged particles spanning the entire energy range. In addition, a TOF (time of flight) with respect to a beam pickoff located upstream of the neutron producing target was used to select only those events associated with the neutrons in the main peak.

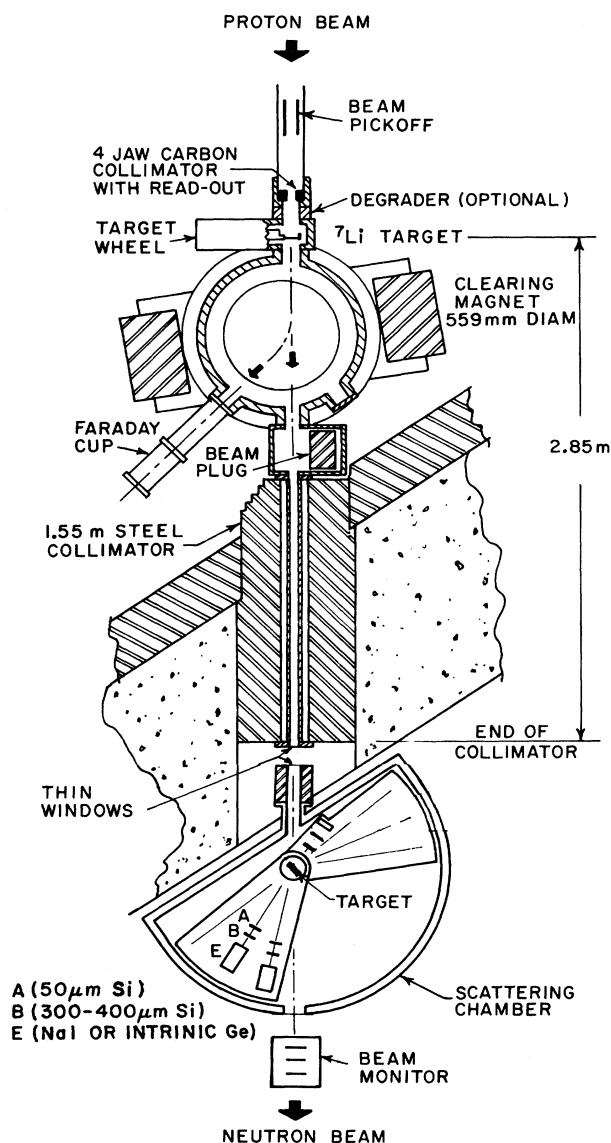


FIG. 1. The unpolarized neutron beam line and the associated scattering chamber at the Crocker Nuclear Laboratory.

Data acquisition was accomplished by feeding the data signals into the PDP 15/40 computer through a CAMAC/CA-15 Branch Driver. The events were characterized by (i) the route or the telescope that registered the event and (ii) the condition as to the element of the said telescope where the particle stopped. Routines provide detailed visual on-line displays for the selected route and/or condition. The raw data were stored event by event on magnetic tape for subsequent retrieval and detailed analysis. See Ref. 5 for a complete description of the experimental setup.

III. DATA REDUCTION

We shall briefly describe the procedure adopted in data reduction. More details can be found in Ref. 5. For each

particle that provides an energy loss in a detector a timing pulse and an energy pulse height were obtained. For particles that passed through at least the first detector, a ΔE vs E scheme was used for particle identification. For those that stopped in the first detector, a time of flight (TOF) vs E scheme was used. In all the cases, a neutron TOF cut was superimposed to select the events given rise to by the neutrons in the peak of the incident neutron beam. When a particle traversed more than one detector the pulse heights from the active detectors were summed after matching their gains.⁸ Corrections for dead layers on detectors were also included. Two sets of energy channels (low and high gain) were provided for each of the ΔE detectors to facilitate better resolution between the helium and hydrogen particles (respectively). Since the helium particles at low energies lost a considerable portion of their energy in the target, these data were corrected for particle and energy loss in the target.⁹ The alpha spectrum for $E < 8$ MeV contains some (not resolved) ^3He contamination produced by the neutron tail (Fig. 2; see also Ref. 5). By comparing the measured ^3He and alpha cross sections in the region around 10 MeV, we estimate this contamination to be $< 5\%$ at 60.7 MeV, $< 3\%$ at 39.7 MeV, and negligible at 27.4 MeV.

The presence of hydrogen in the target necessarily introduces data gaps in the proton energy spectra, owing to the elastic n-p. This effect appears in two ways: the elastic n-p peak from the full energy neutrons, which shifts in energy rapidly with angle (it disappears at 90 degrees), and a low energy gap (it ranges between 2 and 8 MeV) due to the time-of-flight foldover elastic n-p from the neutron tail (Fig. 2).

Absolute cross sections were obtained by normalizing to the n-p elastic cross section using the parametrization of Binstock,¹⁰ our previously measured n-p cross sections,¹¹ and a knowledge of the hydrogen content of the target used. The overall normalization uncertainty is estimated to be 5% (4% for the hydrogen surface density and 3% for the elastic hydrogen peak statistics) compounded with the uncertainty in the n-p cross section [typically 3–5% (Ref. 11)]. The average detector angular resolution was 3° and the neutron beam energy width was ~ 2 MeV.

Correction for background was done by the common "target in" and "target out" runs related by a suitable monitor.

IV. THEORETICAL MODEL

The intranuclear cascade calculations were performed with a code (INCA1) based on the Monte Carlo method outlined by Chen *et al.*¹² It lacks the pion physics of the Chen code, but allows a description of the target nucleus including alpha and, if required, two-nucleon clustering, specified by the spectroscopic factors. It is similar to, though extensively modified from, the code recently described by Mathews *et al.*¹³

In the calculation presented here, the spectroscopic factors are taken from the transformed shell model cluster calculations of Balashov *et al.*¹⁴ [the results of their calculations are in good agreement with experimental spectroscopic factors obtained from (p,p α) (Ref. 15) and (p,pd) (Ref. 16) reactions on ^{12}C]. Thus the ^{12}C nucleus is represented as a time average of 1.64 alpha clusters with

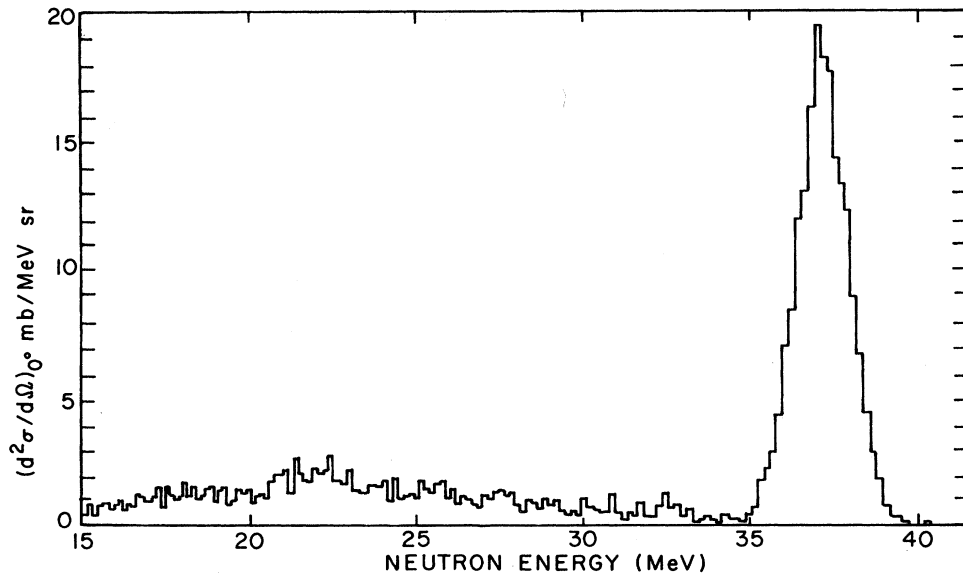


FIG. 2. Typical neutron beam produced by the ${}^7\text{Li}(p,n)$ reaction.

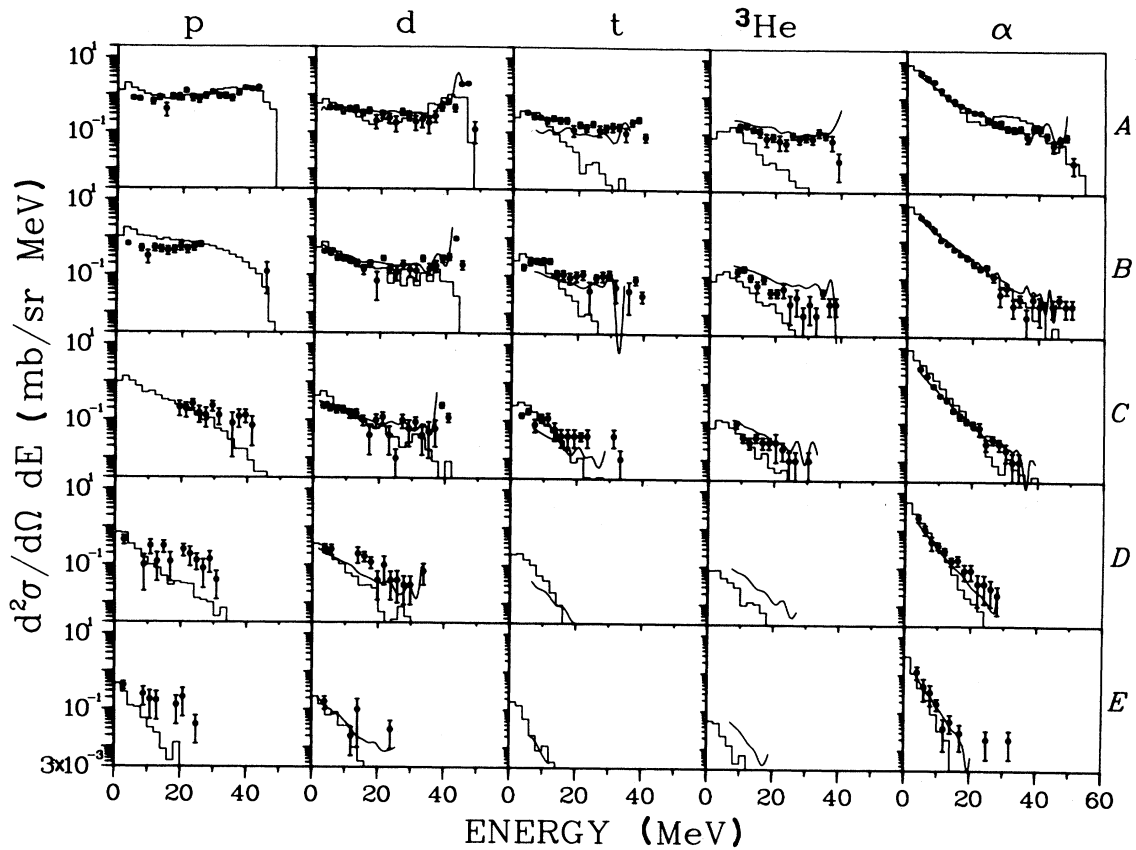


FIG. 3. Results at 61 MeV. For key to plots see Table I. The calculations are shown by a histogram curve. The smooth curves are spline fits to the corresponding charge symmetric proton-induced data obtained by Bertrand and Peelle (Ref. 4). See also Sec. III for the proton spectra.

TABLE I. Key to Figs. 3–5.

	Fig. 3		Fig. 4		Fig. 5	
Energy (MeV)	Neutron experiment	Neutron calculation	Proton experiment	Neutron experiment	Neutron calculation	Proton experiment
	60.7	60.7	61.4	39.7	39.7	38.8
						27.4
						27.4
						28.8
Key						
<i>A</i>	20°	15°–25°	20°	20°	15°–25°	20°
<i>B</i>	40°	35°–45°	40°	40°	35°–45°	45°
<i>C</i>	65°	55°–65°	65°	65°	55°–65°	60°
<i>D</i>	90° ^a	85°–95°	90°	90° ^b	85°–95°	90°
<i>E</i>	150° ^a	145°–155°	150°	150° ^b	145°–155°	130° ^a

^aOwing to experimental constraints prevailing during the data collection run, no data could be extracted for tritons and ^3He at 60.7 MeV, and for deuterons and tritons at 27.4 MeV.

^bNo ^3He above our experimental threshold (8 MeV).

5.44 nucleons. The nuclear density is taken to be uniform in each of 18 radial steps out to 5 fm, with stepwise densities derived from a three-parameter Fermi distribution ($c=2.355$, $z=0.522$, $w=-0.149$).¹⁷ No cluster-cluster interactions are allowed, and secondary particles are allowed to escape freely when the distance from the secondary particle to the center of the nuclear well exceeds an “interaction radius” of $1.07 A^{1/3}$ fm (approximately the half-density radius). The cascade production is restricted by the known one- and two-particle separation energies; by

using the time-interval tracking feature of the code, the particle binding is adjusted to account for previous particle emission and to force conservation of energy in one- and two-particle emission.

Fermi momentum distributions are used for the nucleons, with Fermi energies determined in each spatial region by the nucleon density in that region. Pauli blocking is enforced for scattering of nucleons. To treat the alpha and two-nucleon clusters as bosons, a Fermi momentum distribution appropriate for the density normalized to a

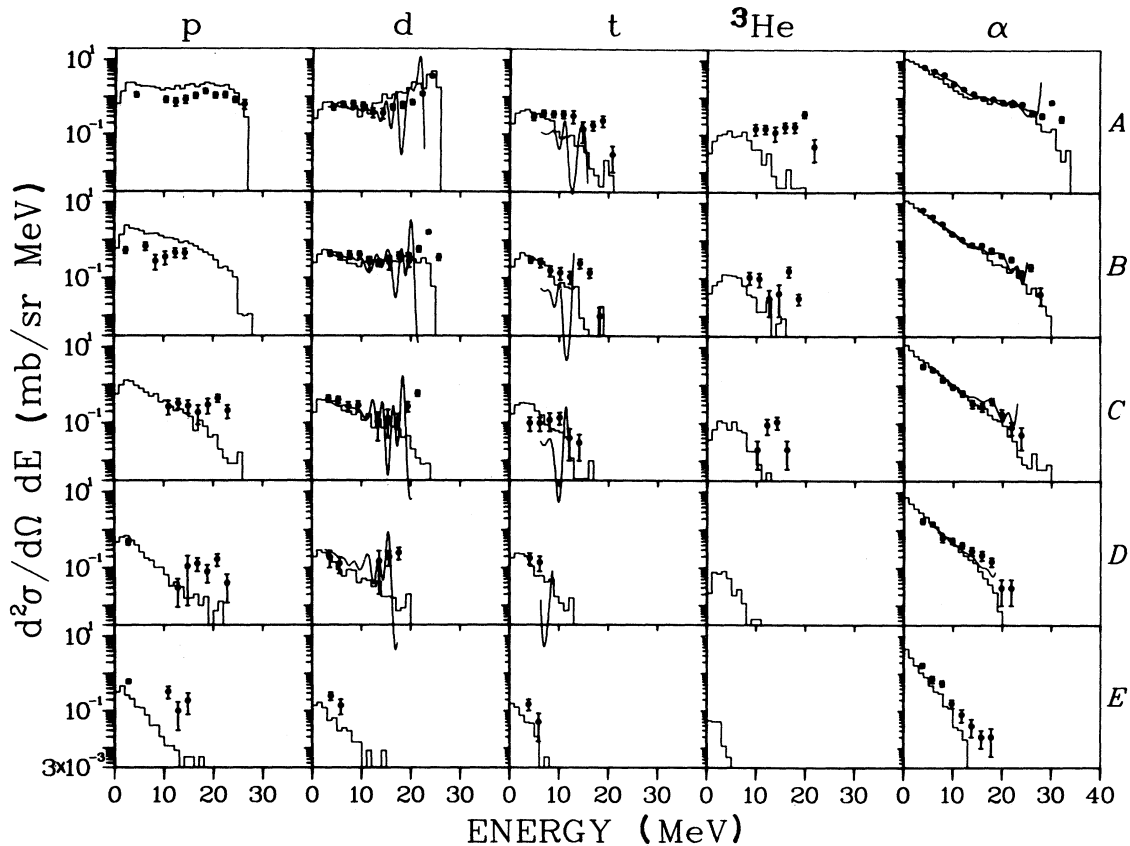


FIG. 4. Results at 40 MeV. Same caption as Fig. 3.

single particle is used.

From kinematic considerations, it is clear that the narrow peak of high energy deuterons that is experimentally observed results from pickup reactions. We have therefore incorporated a simple pickup model as an option in INCA1. Such an approach must be considered somewhat speculative; for though, to first order, on-shell nucleon-nucleon matrix elements may be considered independent of detailed nuclear structure, it is not clear that this is the case for complex-particle interactions. However, the good success obtained by Hachenberg *et al.*¹⁸ using a conceptually similar analytic approach has encouraged us to proceed this way.

The main features of the pickup model are as follows: The energy of the picked-up particle is sampled, as usual, from the Fermi distribution; its direction is determined by conservation of energy and momentum exterior to the nucleus. If the pickup is not allowed by conservation of energy and momentum, the cross section is set to zero; otherwise, it is given by the PWBA expression derived from that given by Selove,¹⁹

$$\sigma_{\text{pickup}} = \frac{\hbar^3}{pp_0^2} |F|^2 \frac{12\pi^2 (\beta^2 - \alpha^2)^2}{1 - \alpha r_e (\beta^2 + q^2)},$$

where p is the momentum of the picked-up particle *within* the nucleus, p_0 is the asymptotic momentum of the incident particle,

$$\hbar q = \frac{1}{2} |\vec{p} - \vec{p}_0|, \quad \beta = 6.2\alpha,$$

and

$$\alpha = \sqrt{ME_B/\hbar},$$

where E_B is the deuteron binding energy (2.225 MeV), M is the nucleonic mass, and r_e is the effective range of the n-p interaction for triplet scattering (1.7×10^{-15} m). $|F|^2$ is a spectroscopic factor that we took from the work of Chew and Goldberger.²⁰ Finally, the asymptotic deuteron momentum is determined by the vector sum of \vec{p}_0 and \vec{p} .

The deexcitation of the residual nuclei is treated by a code (INCA2) using the Fermi breakup model.^{21(a)} The basic model has been described by Epherre and Gradystajn.^{21(b)} In this model channel probabilities and particle momenta are determined by phase-space considerations. However, many features have been added to the model, the most significant of which are as follows:

1. Particle-unstable levels are allowed as intermediate states, thus permitting sequential decay processes.
2. Two-body breakup channels use a Coulomb barrier penetration factor approximated from Coulomb wave functions, while multiparticle modes use a breakup threshold adjusted for Coulomb energy.
3. Two-body breakup of levels with known spin and parity are restricted to conserve parity and isospin and are

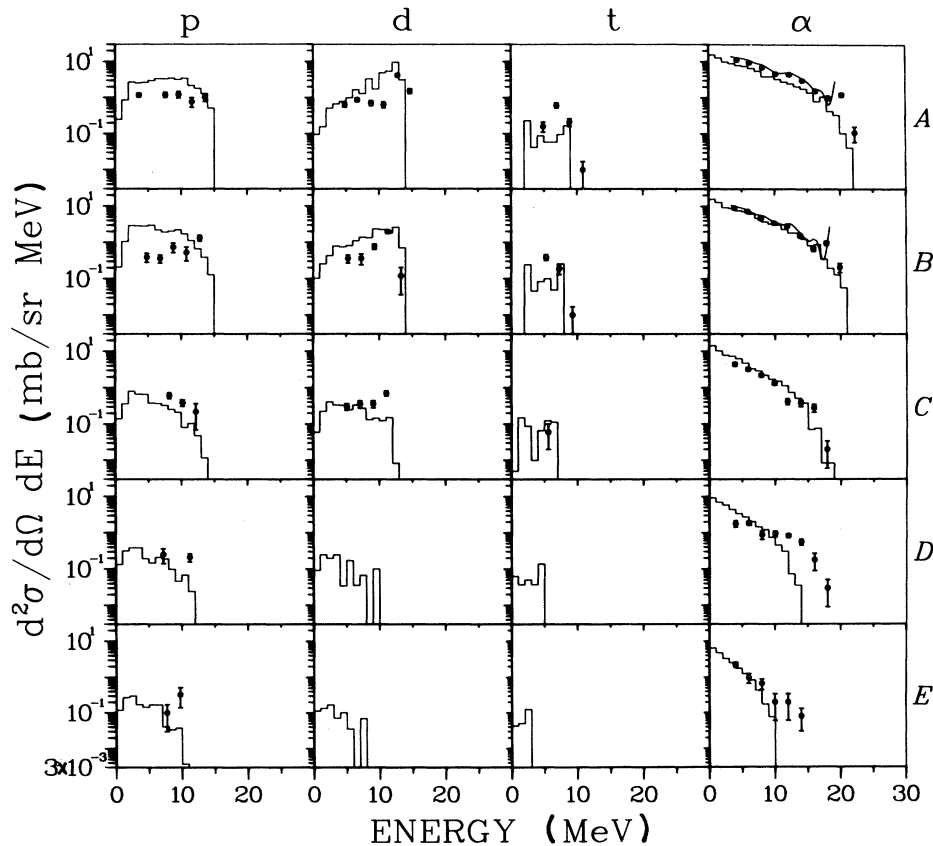


FIG. 5. Results at 27 MeV. Same caption as Fig. 3.

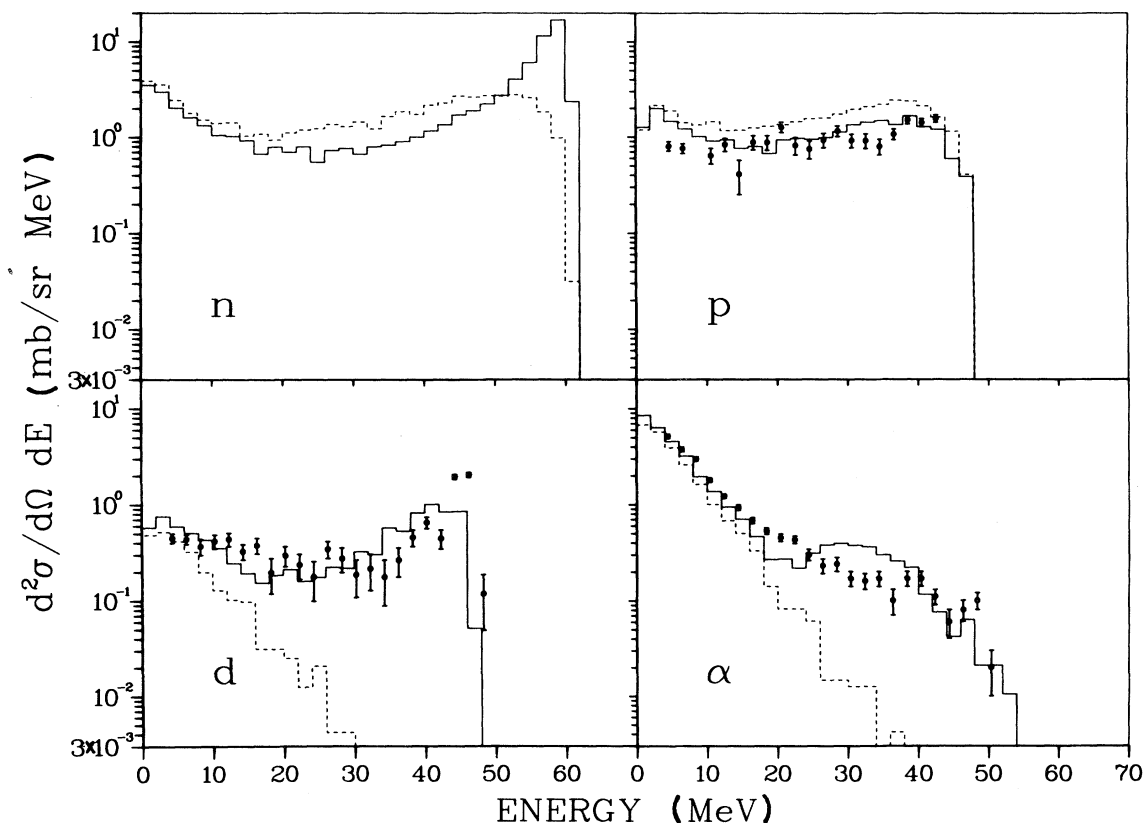


FIG. 6. Comparison of results for neutrons at 60.7 MeV ($15^\circ \rightarrow 25^\circ$) between the calculation including clustering and deuteron pickup (full histogram) and the calculation excluding these options (dashed histogram). The experimental data are shown as points.

inhibited by neutral particle angular momentum barrier penetration factors.

4. Up to seven-body breakup modes are allowed.

5. Experimental data²² are used for mass excesses and for the excitation energies, spins, and isospins, and parities of nuclear levels.

V. DISCUSSION OF RESULTS

A representative selection of experimental and calculated results are shown in Figs. 3–5. For comparison, the corresponding experimental results for proton-induced reactions on carbon obtained by Bertrand and Peelle⁴ are also shown with a spline fit to the data. For the proton-induced data, charge symmetric reactions are compared [(p,xd) with (n,xd) and (p,xα) with (n,xα)] and, hence, the (p,xt) and (p,x³He) are, respectively, compared with the (n,x³He) and (n,xt) reactions. It should be noted that, in order to improve statistics, the theoretical predictions have been averaged over 10° bins, which is considerably broader than the experimental angular resolution of around 3° .

In the calculation, 1.1×10^6 incident neutrons were simulated at each energy. As an indication of the *statistical* error involved, at 39.7 MeV the error in the energy and angle integrated proton production cross section was 0.7%; the error in the angle integrated proton production cross section varied from 1.5% at low proton energy to 7.5% at high proton energy; the error in the double-

differential cross section typically varied from around 8% (low proton energy) to around 12% (high proton energy).

The basic assumption underlying intranuclear cascade calculations is that if the mean free path of a particle inside the nucleus is larger than the distance between the constituent particles of the nucleus, its interactions with these particles may be treated as a series of independent two-body collisions, using free particle cross sections. Although the mean free path of a particle in nuclear matter is hard to define,²³ it is clear that at the energies of the experiment this premise is questionable, and thus the generally good agreement between theory and experiment must be considered somewhat surprising.

For secondary protons, deuterons, and alphas, the calculation generally predicts too few high energy, direct particles at large angles. This is a direct consequence of the two-body interactions used in INCA1. The same reasoning also applies to the deuteron pickup peak which is predicted at rather more forward angles than experimentally observed. In addition, the particular shape of the calculated deuteron peak is a reflection of our assumption of a Fermi momentum distribution for the target nucleons.

The calculations yield few direct nucleons or alphas above $\sim 90^\circ$ and few direct deuterons above $\sim 45^\circ$. Increasing the interaction radius described in Sec. IV results in somewhat more lower energy direct particles at back angles but still fails to predict the high energy particles experimentally observed at large angles. (Increasing the opa-

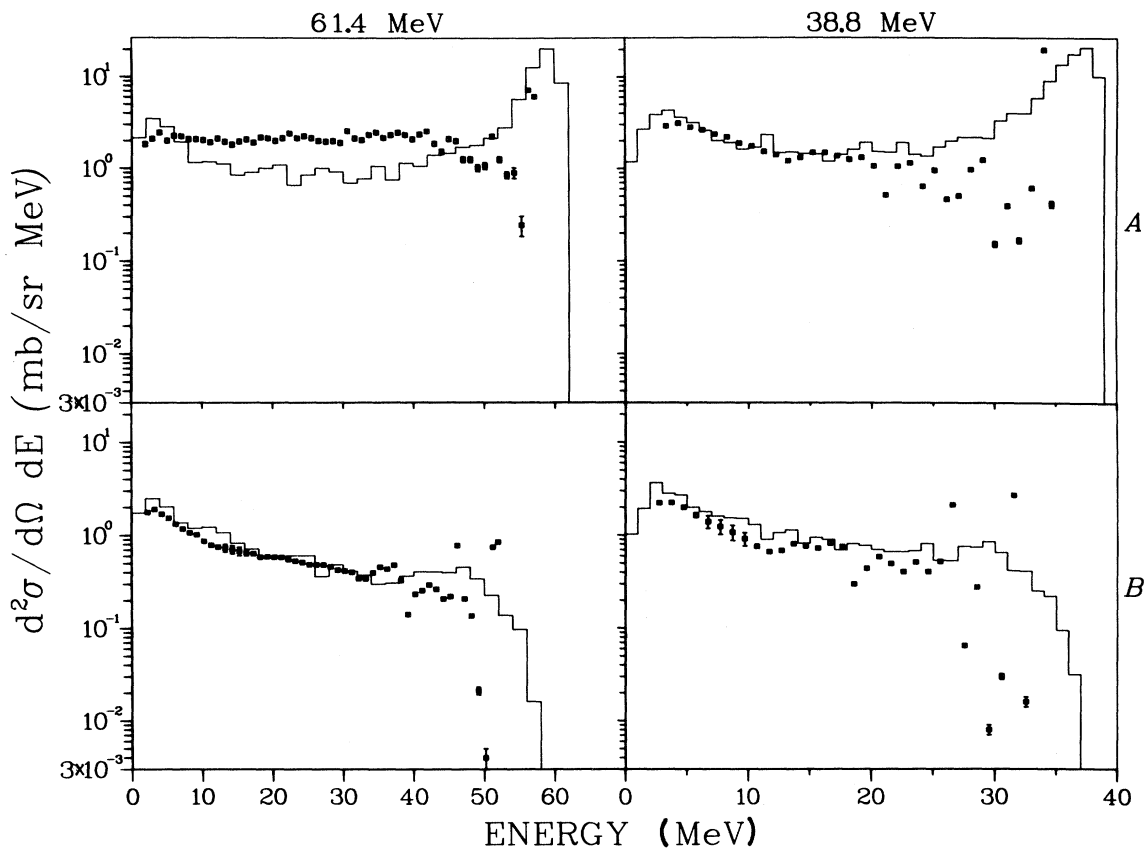


FIG. 7. Calculated secondary proton spectra for 61.4 and 38.8 MeV incident protons (histograms) compared with experimental data of Bertrand and Peelle (Ref. 4). The calculations and experiments on the top row are, respectively, between 15° and 25° and at 20° . The calculations and experiments on the bottom row are, respectively, between 55° and 65° and at 60° .

city of the nucleus in this way would, however, reduce the excessive number of low energy protons that are predicted.) It would not seem possible, within the context of a classical "direct reaction + compound nucleus" model²⁴ to predict these high-energy large angle particles and it would appear, within this context, that they are produced during an intermediate regime before statistical equilibrium is obtained.

The effects of particle clustering and of the deuteron pickup formalism are illustrated in Fig. 6, where the dashed lines are the results of a calculation including neither of these options. The high-energy peak in the secondary neutron spectrum when they are included is due to the reduction of high momentum transfer neutron-nucleon scattering and an increase in low momentum transfer neutron-cluster scattering. In addition, the intermediate and high energy neutron and proton spectra are reduced due to competition from the pickup reaction. From the deuteron and alpha spectra it is clear that agreement cannot be obtained without the assumption of deuteron pickup and alpha clustering. Returning to Figs. 3–5 it is also apparent that particle transfer yielding tritons and ^3He is occurring; these reactions have not, however, been modeled in our code.

Considering the proton-induced data of Bertrand and

Peelle,⁴ the agreement shown in Figs. 3–5 for all comparable particles, energies, and angles confirms the expected similarity between cross sections for reactions induced by protons and neutrons in self-conjugate nuclei. The corresponding theoretical predictions are also very similar, showing slight differences primarily due to the different particle separation energies. The proton-induced data allow also for a comparison of experimental (N, xN) data with our calculations. Some typical comparisons are shown in Fig. 7 for two incident energies and two angles. At small angles the calculation overpredicts at high energies and underpredicts at intermediate energies, an effect which would be decreased by increasing the opacity of the nucleus, as described above. At larger angles, however, the high energy peak due to clustering is absent and the agreement is much improved.

Finally, it should be noted that the calculation does not reproduce the high energy structure observed by Bertrand and Peelle⁴ for the (p,xp) data in Fig. 7. This is because the *direct* (INC) part of the calculation does not use the experimental nuclear level data, and thus the only way for level structure to appear in our calculated results would be from a second nuclear deexcitation from one given level to another. Thus *direct* nuclear reactions yielding a given excited state are not simulated.

VI. CONCLUSIONS

We have obtained the first comprehensive set of inclusive hydrogen and helium double-differential spectra after neutron bombardment of carbon. The data have been compared with the corresponding proton-induced results yielding good agreement and with intranuclear-cascade—Fermi-breakup calculations. Comparisons with these calculations are in general favorable but clearly show the limitations of the model.

Only a representative selection of results have been shown here. Full details of the experimental results at all angles may be obtained from J. L. Romero. Microfiche containing detailed results of the calculations, including kerma factors, at incident neutron and proton energies be-

tween 10 and 150 MeV for carbon, nitrogen, and oxygen, may be obtained from D. J. Brenner or R. E. Prael. Further experimental results for nitrogen and oxygen will be presented in further publications.

ACKNOWLEDGMENTS

We would like to thank E. Russell, J. McCurdy, and the Crocker Nuclear Laboratory crew for providing a variety of beams in the preparatory and the executional phases of this experiment. We also thank Dr. Vic Viola and Dr. Ali Gökmen for sending us the original version of INCA1. We acknowledge the support of the National Cancer Institute, Grant CA-16261, and the National Science Foundation, Grants PHY71-03400 and PHY77-05301.

*Present address: The Radiation Oncology Center for Northern Illinois, Swedish American Hospital, Rockford, IL 61101.

† Present address: Department of Physics, Kent State University, Kent, OH 44242.

‡ Present address: Department of Physics, University of California at Los Angeles, Los Angeles, CA 90007.

§ Permanent address: Department of Physics, University of Auckland, Auckland, New Zealand.

|| Present address: Rocketdyne Division, Rockwell, Canoga Park, CA 91304.

¶ Present address: Nuclear Physics Laboratory, University of Colorado, Boulder, CO 80309.

¹Proceedings of the Symposium on Neutron Cross Sections from 10–50 MeV, edited by M. R. Bhat and S. Pearlstein, Brookhaven National Laboratory Report No. BNL-NCS-51245, 1980 (unpublished).

²J. F. Londe, J. P. Perroud, and Ch. Sellem, *Helv. Phys. Acta.* **44**, 33 (1971); B. Antolkovic and Z. Dolenc, *Nucl. Phys.* **A237**, 235 (1975); E. A. Davis, T. W. Bonner, D. W. Worley, Jr., and R. Bass, *ibid.* **48**, 169 (1963).

³D. A. Kellog, *Phys. Rev.* **90**, 224 (1953).

⁴F. E. Bertrand and R. W. Peelle, *Phys. Rev. C* **8**, 1045 (1973); Oak Ridge National Laboratory Report No. ORNL-4799, 1973.

⁵T. S. Subramanian, J. L. Romero, and F. P. Brady, *Nucl. Instrum. Methods* **174**, 475 (1980).

⁶J. A. Jungerman and F. P. Brady, *Nucl. Instrum. Methods* **89**, 167 (1970).

⁷We are thankful to Dr. Fred Bertrand for providing the CH targets.

⁸The gains for the surface barrier Si detectors were determined using the 5.48 MeV α from the ²⁴¹Am source. The NaI (Tl) detectors were calibrated with the elastically scattered forward angle proton peaks.

⁹M. L. Johnson, J. L. Romero, T. S. Subramanian, and F. P. Brady, *Nucl. Instrum. Methods* **169**, 179 (1980).

¹⁰J. Binstock, *Phys. Rev. C* **10**, 19 (1974).

¹¹T. C. Montgomery, F. P. Brady, B. E. Bonner, W. B. Broste, and M. W. McNaughton, *Phys. Rev. Lett.* **31**, 640 (1973); *Phys. Rev. C* **16**, 499 (1977); N. S. P. King, J. D. Reber, J. L. Romero, D. H. Fitzgerald, J. L. Ullmann, T. S. Subramanian, and F. P. Brady, *ibid.* **21**, 1185 (1980).

¹²K. Chen, Z. Fraenkel, G. Friedlander, J. R. Groves, J. M. Miller, and Y. Shimamoto, *Phys. Rev.* **166**, 949 (1968).

¹³G. J. Mathews, B. G. Glagola, R. A. Moyle, and V. E. Viola, Jr., *Phys. Rev. C* **25**, 2181 (1982).

¹⁴V. V. Balashov, A. N. Boyarkina, and I. Rotter, *Nucl. Phys.* **59**, 417 (1964).

¹⁵P. G. Roos, N. S. Chant, A. A. Cowley, D. A. Goldberg, H. D. Holmgren, and R. Woody III, *Phys. Rev. C* **15**, 69 (1977).

¹⁶J. Y. Grossiord, M. Bedjidian, A. Guichard, M. Gusakow, J. R. Pizzi, T. Delbar, G. Gregoire, and J. Lega, *Phys. Rev. C* **15**, 843 (1977).

¹⁷C. W. DeJager, H. de Vries, and C. de Vries, *At. Data Nucl. Data Tables* **14**, 479 (1976).

¹⁸F. Hachenberg, H. C. Chiang, and J. Hüfner, *Phys. Lett.* **97B**, 183 (1980).

¹⁹W. Selove, *Phys. Rev.* **101**, 231 (1956).

²⁰G. F. Chew and M. L. Goldberger, *Phys. Rev.* **77**, 470 (1950).

²¹(a) E. Fermi, *Prog. Theor. Phys.* **5**, 570 (1950); (b) M. Epherre and E. Gradystajn, *J. Phys. (Paris)* **28**, 747 (1967).

²²S. Fiarman and S. S. Hanna, *Nucl. Phys.* **A251**, 1 (1975); **A206**, 1 (1973); F. Ajzenberg-Selove, *ibid.* **A320**, 1 (1979); **A335**, 1 (1980).

²³E. Gadioli, E. Gadioli Erba, G. Tagliaferri, and J. J. Hogan, *Phys. Lett.* **65B**, 311 (1976); M. Blann, *ibid.* **67B**, 145 (1977).

²⁴R. Serber, *Phys. Rev.* **72**, 1114 (1947).